

Electron paramagnetic resonance study of type-II silicon clathrate with low sodium guest concentration

William K. Schenken,¹ Yinan Liu ², Lakshmi Krishna,¹ Ahmad A. A. Majid,² Carolyn A. Koh,^{2,*} P. Craig Taylor ¹ and Reuben T. Collins¹

¹Department of Physics, Colorado School of Mines, Golden, Colorado 80401, USA

²Department of Chemical and Biological Engineering, Colorado School of Mines, Golden, Colorado 80401, USA



(Received 12 December 2019; revised manuscript received 15 May 2020; accepted 3 June 2020; published 22 June 2020)

An electron paramagnetic resonance (EPR) study of type-II silicon (Si) clathrate with low sodium (Na) guest concentration provides insights into the properties of this cagelike Si allotrope and into Na as an n -type dopant. An EPR line arising from unterminated Si bonds in a disordered Si phase is identified in the system. The presence of this amorphouslike component helps explain the thermally activated, hopping-related conductivity that has long been observed in the system but which has been poorly understood. This study also identifies “superhyperfine” lines surrounding each Na hyperfine line due to interactions of the donor electron with a ^{29}Si nucleus on the cage and confirms the identification of hyperfine lines due to interactions of two neighboring Na nuclei. Analysis of the strength of these interactions shows that the electron wave function associated with the Na donor extends onto surrounding cages consistent with identification of Na as a shallow donor, and provides quantitative evidence of Na clustering.

DOI: [10.1103/PhysRevB.101.245204](https://doi.org/10.1103/PhysRevB.101.245204)

I. INTRODUCTION

Silicon (Si) clathrates are cagelike, crystalline Si inclusion compounds [1]. Room-temperature and atmospheric pressure metastable clathrates are synthesized in the presence of alkali-metal guest atoms, such as sodium (Na), which occupy the interstitial sites in the cages [2,3]. Na guests, however, degenerately dope the crystals [4–6]. If the Na concentration can be reduced well below the metal-insulator transition, the clathrates effectively become new semiconducting Si allotropes with potentially exciting optoelectronic properties. For example, a band gap near 1.9 eV has been reported for type-II Si clathrate and direct or nearly direct band gaps have been predicted theoretically for SiGe clathrate alloys [7–11]. Realizing this potential requires fundamental understanding of guest properties and how to control their occupancy and diffusion in the cagelike host crystal structure. Elucidation of the properties of the Na guest is complicated by a lack of understanding of the defect structure of the Si framework and complex interactions among the Na donors, making experimental results such as the temperature dependence of conductivity difficult to interpret [3,4].

Si clathrates can be formed in either type-I ($\text{Na}_8\text{Si}_{46}$) or type-II ($\text{Na}_{24}\text{Si}_{136}$) structural variations [1,12]. The removal of Na has been achieved to a much greater extent in type II, and so type II is typically written as $\text{Na}_x\text{Si}_{136}$ where x values less than 0.01 have been achieved [3,5,11]. For this reason, type II has received more attention than type I in the literature, and is the focus of this study. The first report of the synthesis and characterization of Si (and Ge) type-II

clathrate structures from thermal decomposition of alkali-metal silicides appeared in 1970 [2]. The final material was a powder, and the characterization techniques included measurements of the low-temperature electrical conductivity as a function of Na concentration. Very soon after this initial discovery, Mott argued that the electrical conductivity in type-II silicon clathrate at low Na concentration was dominated by an “amorphous region” that existed between the individual Si clathrate grains leading to a conductivity controlled by thermally activated hopping (so-called $T^{-1/4}$ behavior) [4]. To date, although almost all reports of electrical conductivity in type-II Si clathrate are consistent with transport that is limited by this highly disordered phase, conflicting interpretations, mainly from the electron paramagnetic resonance (EPR) experiments reported to date, have done little to identify the defects controlling the conductivity [3–5,13,14].

A few studies overcame these difficulties with different material synthesis techniques, and produced the expected conductivity trends in powdered samples for samples with low [11] and high [15] Na concentration. There have also been multiple reports of single-crystal synthesis of Si clathrates, where effects due to grain surfaces would not be present [16–19]. These studies allowed for an investigation of intrinsic transport properties, such as the observation of the metal-insulator transition around $x \sim 8$ [19].

EPR studies have also been directed at understanding the properties of the Na guests. A line attributed to conduction electrons donated by the Na has been reported [3,13]. For lower Na concentration ($\text{Na}_x\text{Si}_{136}$ with $x < 5$) and at low temperature (< 200 K), the EPR spectrum of type-II Si clathrates exhibits four nearly evenly spaced hyperfine lines due to the interaction of the Na’s valence electron with its nucleus [3,5,13,14]. The atomic hyperfine coupling constant for an s

*Corresponding author: ckoh@mines.edu

electron on Na has been used to estimate that roughly 42% of the donor electron resides on the Na nucleus with the rest on or beyond the Si cage, while additional fine structure has been attributed to clusters of Na atoms [5,13,20].

Here, we report an EPR study of type-II Si clathrate prepared with very low Na concentration. We attribute a previously unidentified EPR line to a silicon atom in a tetrahedral environment with a missing nearest neighbor, which in amorphous silicon is usually termed a “dangling bond.” Details of this identification suggest that these defects arise from the elusive highly disordered phase that surrounds the Si clathrate grains and controls the low-temperature conductivity. We also identify subtle “superhyperfine” doublets surrounding each of the Na hyperfine lines which arise from interactions with naturally occurring ^{29}Si in the large cages. These lines provide a new probe of the extension of the Na valence electron past the Si cage and reinforce the view of Na interstitials as shallow donors in type-II Si clathrate. We also confirm that fine structure lying between the Na hyperfine lines arises from Na donor pairs. The strength of these features suggests that the distribution of Na atoms in the cages is not random and possible explanations for this “clustering” are discussed. Taken together these results resolve long-standing confusion about electron transport in type-II Si clathrates and reinforce the notion that, at low Na concentration, Si clathrates could become an interesting, alternative *n*-type crystalline Si-based semiconductor.

II. EXPERIMENT

The powder clathrate samples used in this study were prepared by a synthesis process that results in a high fraction of type-II material and low Na concentration as discussed in detail in Ref. [3]. Here, we give a brief overview of the synthesis. NaH (95%, Aldrich) and Si (99.9999%, Alfa Aesar) powders in the ratio of 1.6:1 were ball-milled together. The resulting powder was loaded into a covered alumina crucible boat and heated at 395 °C (668 K) under flowing Ar for 48 h to form NaSi. Excess Na was removed from the resulting NaSi by annealing for 3 h at 250 °C (523 K) under dynamic vacuum. Finally, the NaSi powder was decomposed into clathrate by heating under dynamic vacuum at 370 °C (643 K) for 3 days in a conventional tube furnace or in a reactor with a cold plate located near the sample. With the latter, the Na condensed onto the cold plate holding the vapor pressure low and resulting in mostly type-II clathrate. Following the synthesis, the samples were etched in an HF/HNO₃ in water solution for 1–15 min, lowering the Na concentration and the type-I phase [3]. The reduction in Na may be due to selective etching. More heavily doped conventional diamond Si exhibits a higher etch rate in HF/HNO₃ solution [21]. Since type-I clathrate tends to retain the Na guests more than type II, as previously mentioned, it is likely to be more highly doped leading to faster etching of type I than type II. This approach leads to Na concentrations below the lower limit that can be detected using x-ray diffraction ($x < 0.5$) [3]. 5–25 mg of this material were then sealed under vacuum in a 5-mm-diameter quartz tube for the EPR measurements. Reference [3] presented EPR results and a brief discussion of the spectra for several samples prepared in this manner. This

paper provides an in-depth analysis of the samples with the lowest Na concentration.

In addition, a hydrogenated amorphous silicon (*a*-Si:H) sample was studied to compare portions of the EPR spectrum to that of the type-II Si clathrate. The *a*-Si:H deposition occurred on an aluminum foil substrate held at 200 °C (473 K) in a PECVD chamber with capacitively coupled, RF electrodes that were 15 mm apart. The precursor was pure silane with a flow rate of 20 sccm. Chamber pressure was held at 500 mTorr. The applied RF power was 1 W at 13.56 MHz. Following the growth, the sample was placed in dilute HCl (6 M) for 20 min which etched the aluminum, removing the substrate. The resulting solution was passed through filter paper to separate the *a*-Si:H from the solution and rinsed in water. The resulting powder was transferred to a quartz tube and sealed under vacuum. The final sample weighed roughly 5 mg.

Samples were studied using an X-band Bruker EMX EPR Spectrometer. The microwave frequency was measured with an EIP 548 A Microwave Frequency Counter, and the magnetic field was calibrated using the known $g = 2.0028$ EPR line of a strong pitch (0.1% pitch in KCl) sample as a reference. The magnetic field modulation amplitude for each sample was 1 G such that linewidths are directly comparable. Other parameters were adjusted to optimize the signal for the specific sample, as discussed in the figure captions. Spin densities were obtained by comparison of the doubly integrated EPR spectrum to either strong pitch or weak pitch (0.00033% pitch in KCl) reference samples measured with the same parameters. A continuous flow dewar insert allowed temperature-dependent measurements. For *a*-Si:H, only room temperature and 100 K were measured. The spin density obtained for the *a*-Si:H sample was $\sim 10^{16}$ cm⁻³. At this spin density and over this temperature range, *a*-Si:H is well understood to follow a paramagnetic Curie law. The observations made at room temperature and 100 K were consistent with the known behavior as described in Ref. [22]. Measurements of type-II clathrate were made at eight different temperatures from room temperature down to 10 K, and the spin densities obtained are discussed later in the text.

III. RESULTS

A. Room-temperature results

Figure 1 shows a comparison of the EPR spectra of the *a*-Si:H sample and the type-II Si clathrate sample at room temperature. The *a*-Si:H spectrum, which exhibits a g value of 2.005 and is attributed to unterminated Si bonds, was scaled to match the peak of the clathrate spectrum to compare line shapes. The difference between the two spectra is shown in blue.

The subtracted spectrum exhibits very little residual signal at fields below 338 mT. The line that remains after subtraction has a g value of 2.003 as expected for conduction electrons. The identification of the residual with conduction electrons is further supported by the reduction of the intensity of this feature with decreasing temperature, as described in more detail in the next section, consistent with carriers in the conduction band becoming localized on the Na atoms. Moreover,

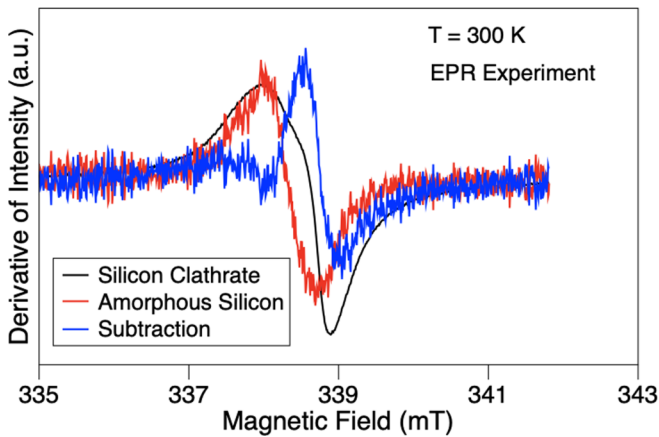


FIG. 1. Room-temperature comparison of the low Na Si clathrate with *a*-Si:H and their subtraction. The *a*-Si:H spectrum was averaged over 75 scans with 1024 data points, an acquisition time of 35 ms per data point, a gain of 10^4 , and 1.08 mW microwave power. The clathrate spectrum was taken over 5 scans with 1024 data points, an acquisition time of 30 ms per data point with a gain of 10^3 , and 1.08 mW microwave power. Each curve is adjusted to the same microwave frequency. The *a*-Si:H curve was scaled vertically to compare qualitative features between the two spectra.

temperature-dependent measurements of the clathrate EPR spectrum show that the line at $g = 2.005$ scales with temperature according to the paramagnetic Curie law, consistent with the temperature dependence expected and observed for the nearly isolated spins in amorphous silicon.

The information given above allows us to conclude the room-temperature spectrum is a superposition of the dangling bond defect line at $g = 2.005$ and a free-carrier feature arising from Na donors. Similar conclusions are reached by direct fitting of the clathrate spectrum to *a*-Si:H and free-carrier EPR spectra. We have applied the same analysis to a range of clathrate samples prepared with different Na concentrations and find the same decomposition into dangling bond and free-carrier lines fits all of the spectra at room temperature. A search of the literature shows that most, if not all, EPR spectra of powder synthesized type-II Si clathrate samples exhibit a feature consistent with the dangling bond signature identified here [3,5,13,14].

Comparing the integrated intensity of the dangling bond signal in the clathrate spectrum in Fig. 1 to that of a strong pitch reference acquired using the same parameters yields a spin density of $\sim 2 \times 10^{17} \text{ cm}^{-3}$. The dangling bond density in amorphous silicon is a strong function of the concentration of hydrogen which terminates dangling bonds. The low defect density of our amorphous silicon sample is the result of hydrogen passivation. In contrast, the only hydrogen introduced in our clathrate preparation occurs at the first step and subsequent processing temperatures are too high for it to remain in the clathrate. The spin density of $\sim 2 \times 10^{17} \text{ cm}^{-3}$ we observe in our clathrate sample is consistent with, but at the low end of, the defect density of amorphous silicon prepared without hydrogen passivation [23]. This density assumes that the defects are uniformly distributed throughout the material. As discussed below, we suspect they are located in a smaller

shell of disordered material at the surface of the grain and that the actual density is larger.

As a consistency check, we have examined the saturation of the intensity of the dangling bond EPR signal at low temperature. In amorphous silicon, exchange interactions cause the saturation behavior to vary with defect density. For example, at temperatures below 40 K, the signal intensity in hydrogenated amorphous silicon with a low density of paramagnetic centers saturates at microwave power levels much lower than those used here, becoming essentially undetectable relative to other features in the spectrum. This happens because the spin-lattice relaxation time increases at low temperature. This is the behavior we observe in the amorphous silicon sample prepared for this study.

In highly defective *a*-Si this relaxation is much faster [24] leading to less saturation and allowing the dangling bond line to be observed at low temperature. The fact that we can see this line at low temperature in Fig. 1 is an indication of a high density of dangling bonds. The temperature dependence of the saturation of the dangling bond line in our clathrate powders is typical of *a*-Si with a defect density of $\sim 10^{18} \text{ cm}^{-3}$.

Based on these results, we attribute the dangling bond feature to the presence of a disordered Si phase like amorphous Si. We speculate that the phase is primarily located at the surface of individual grains creating a bottleneck in grain-to-grain transport that gives rise to the thermally activated hopping conductivity that has been observed in many studies of pressed powders. This view of a surface contribution is consistent with the reduction in the dangling bond signal relative to the free carrier and hyperfine related lines we observe after the HF/HNO₃ etch, which would preferentially effect grain surfaces. See Fig. S1 in the Supplemental Material [25] for a demonstration of the effects of etching in our samples. Related observations were reported by Ammar *et al.* [5] where repeated treatments with elemental iodine at 300 °C–400 °C tended to reduce the intensity of the line at $g = 2.005$. Iodine is known to passivate defects in Si within this temperature range [26,27], though the atomic radius of iodine is too large compared to the spacings in the silicon lattice for the iodine to passivate dangling bonds much deeper than the surrounding shell. Thus, their results can be interpreted as the passivation of dangling bonds located near the surface of the individual grains. While we have identified the dominant defect in this phase, the exact structural nature of the disordered layer remains an open question. Given the comparisons we have made to amorphous silicon, it would not be surprising if it were composed of an amorphous silicon layer. Other options are possible, however, such as a highly defective clathrate skeleton surrounding a crystalline clathrate core.

B. Low-temperature results

A low-temperature (10-K) EPR spectrum of type-II Si clathrate with low Na concentration (≤ 1 at. % Na) is shown in black in Fig. 2. It exhibits a great deal of fine structure which can be identified through simulations obtained using the EASYPIN software [28]. The clearest feature in the spectrum is the four EPR lines arising from hyperfine interactions between the Na nucleus ($I = \frac{3}{2}$) and the valence electron, now lying in a localized donor state within the crystal. As shown in

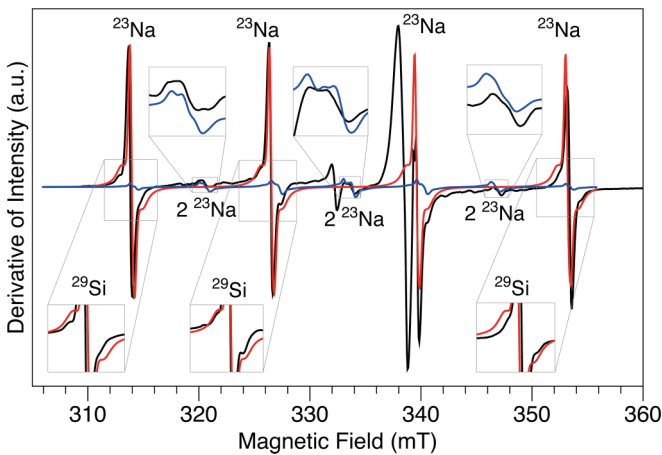


FIG. 2. (Black) Experimental EPR spectrum of one of the lowest Na content samples at 10 K. (Red) Sum of calculated EPR spectra consisting of an electron interacting with a single Na nucleus and n ^{29}Si on the surrounding cage ($n = 0, 1, \text{ and } 2$). (Blue) Sum of calculated spectrum for two Na nuclei. Insets show the details of the two-sodium related structure (above) and of the ^{29}Si splittings (below). Details are discussed in the text, and parameters for the experimental data are given in Ref. [3].

Fig. 2, these hyperfine lines lie at 314, 326, 339, and 353 mT for the given frequency. The line at 339 mT is somewhat obscured in the measured spectrum by the dangling bond and free-carrier signals which are still present at low temperature as discussed in more detail below. Our EASYSYSPIN simulations of the hyperfine lines use an isotropic hyperfine coupling constant for Na of 13.3 mT as reported by several authors [3,5,13,14]. Roy *et al.* [14,20] presented a rough calculation for the donor wave function using this coupling. They found that roughly 42% of the probability distribution lies within the cage, while the rest (about 58%) resides on or extends past the surrounding Si sublattice. There exists a small anisotropy in the four hyperfine lines in Fig. 2, which is captured by the calculated data using axially symmetric g values of 2.0385, 2.0385, and 2.0360. The assignment of the anisotropy to the g tensor is supported by the similar linewidths and intensities of the hyperfine lines, as shown in Fig. S2 in the Supplemental Material [25]. The anisotropy indicates that the Na atom is slightly off center in the large cage, as suggested by other measurements [15,16,29–32].

The blowups shown in the insets at the bottom of Fig. 2 reveal small doublets surrounding each of the ^{23}Na hyperfine lines. These features are reproducible in our work. They are even visible in prior published spectra [5,13] although they were not identified or discussed. We identify these features as “superhyperfine” lines resulting from interactions of the unpaired Na donor electron with ^{29}Si nuclei, which have spin $\frac{1}{2}$, on the surrounding cage. An EASYSYSPIN simulation shown in red in Fig. 2 which takes into account the statistical variation in the number of ^{29}Si atoms on a cage assists with this identification. This variation is modeled in the simulation using a binomial distribution and the natural abundance of ^{29}Si , 0.0467, to determine the probability that a given large cage has “ n ” ^{29}Si atoms on the 28 sites that make up the cage. For example, the probability that there are no ^{29}Si

atoms on the cage is $(1-0.0467)^{28} = 26.2\%$. See Table S1 in the Supplemental Material [25] for the details of this calculation.

To simulate the EPR spectrum for this system, we first calculated individual spectra composed of one electron, a single Na nucleus, and n ^{29}Si atoms. We then multiplied each spectrum by its respective probability, and summed the spectra. This was done for $n = 0, 1, \text{ and } 2$. Contributions for $n \geq 3$ were too small to be visible. In this approach, the main hyperfine line arises from cages with no ^{29}Si atoms with a smaller additional contribution from cages with two ^{29}Si atoms. The linewidth for the $n = 0$ contribution was determined by fitting to the width of the observed Na hyperfine line. To fit the ^{29}Si superhyperfine structure, a linewidth roughly three times larger was used for $n = 1$ and six times larger for $n = 2$. An increase in the linewidth is reasonable. Consider as an example the $n = 1$ case which gives rise to the superhyperfine doublet. The separation of the doublet is determined by the coupling constant which depends on the amplitude of the donor electron wave function at the ^{29}Si site. For the large cage of a Si clathrate, there are three inequivalent Si sites which will give rise to variation in the coupling constant and inhomogeneous broadening of the linewidth. While we feel ^{29}Si atoms on the cage immediately surrounding the Na donor are primarily responsible for the doublet, any contribution from a ^{29}Si on a next-nearest-neighbor cage would only add to the broadening. The same argument has been used to explain the decrease in the linewidth of the ^{31}P hyperfine line in diamond silicon as the ^{29}Si isotope concentration is reduced [33]. In this case, the P donor wave function extends over many different lattice sites and so many different ^{29}Si separations that the superhyperfine structure manifests itself as more than an order of magnitude increase in linewidth for naturally occurring Si relative to isotopically purified material [33].

The observation of ^{29}Si related fine structure confirms that the electronic wave function of the donor electron on the ^{23}Na has significant amplitude on the surrounding Si cage. The ^{29}Si coupling constant obtained from the EASYSYSPIN fit to the spectrum is 2.0 mT. We can use the magnitude of the ^{29}Si interaction to make another estimate of how far the wave function extends onto the Si sublattice. Considering one ^{29}Si on a large cage, which accounts for the doublet in the EPR spectrum, we can use the fraction of ^{29}Si atoms (1/28), the ^{29}Si atomic coupling constant of 122 mT [34,35], and the charge density of the paramagnetic electron on the Si sublattice (58%) obtained from the ^{23}Na hyperfine interaction discussed above to make a prediction for the ^{29}Si coupling constant of 2.5 mT, which we would observe if the fraction of the electron spin density that extends onto the Si sublattice is only localized on the Si cage surrounding the Na atom. Comparing this to the coupling constant obtained from our fit, we estimate that about 20% of the spin density on the Si sublattice extends past the confining cage and into neighboring cages.

A second EASYSYSPIN simulation was used to assist in identifying the fine structure that lies between the ^{23}Na hyperfine lines, which is highlighted in the upper insets in Fig. 2. The simulation shown in blue in Fig. 2 assumes the presence of two Na atoms and two associated donor electrons. The

simulation takes into account the presence of ^{29}Si . As with a single Na nucleus, spectra weighted by the probability a given number of ^{29}Si atoms were present were summed. In this case, however, any ^{29}Si related structure was so small that essentially the same spectra would have been obtained by ignoring its presence.

The simulation calculated energy eigenstates for the Na donor pair using the same Hamiltonian used in previous studies of P donor pairs in diamond Si [36,37]. The key parameters for the calculation include the Zeeman energy, the Na hyperfine coupling, and exchange coupling which arises from the presence of the two spin- $\frac{1}{2}$ electrons. The former were obtained from the prior fit to the single Na hyperfine structure. To best fit the spectrum, an exchange coupling which was comparable to or larger than the hyperfine and Zeeman terms was required. In this limit, the spectrum was insensitive to the value of the exchange [36,37].

The simulation in Fig. 2 consists of seven lines due to the seven possible spin orientations of the two Na nuclei. In an experimental spectrum, four of the seven lines would be hidden by the four strong hyperfine lines from isolated ^{23}Na . The remaining weak peaks around 321, 334, and 347 mT are due to the interaction with two Na nuclei. This fine structure has previously been observed and variously attributed to the sodium dimer Na_2^+ with two Na atoms residing in a single cage [13], two Na atoms in adjacent cages, or to forbidden transitions [3]. The excellent fit to the structure we observe here suggests that it does arise from the presence of two Na atoms in close proximity. From our EPR measurements alone we cannot distinguish two Na atoms in the same cage from two Na atoms in neighboring cages. There are, however, other studies which suggest the latter is the correct view. Magnetic susceptibility measurements of high Na samples ($\text{Na}_{30.5}\text{Si}_{136}$) suggested the existence of two Na atoms in the same cage, as the susceptibility decreased with decreasing temperature, consistent with the transition of Na_2^+ to the Na_2 molecule at low temperature [38]. However, this trend went away as the sodium content was lowered from $x = 30.5$ to 24, suggesting Na_2 molecules only form under sufficiently high Na concentrations. Additionally, extended x-ray absorption fine structure (EXAFS) measurements of $\text{Na}_8\text{Si}_{136}$ (where only the large cages are filled) suggested the formation of pairs in adjacent cages [31].

The spectral region that includes the disordered silicon and free-carrier signals given in Fig. 1 can be examined at low temperature by expanding the spectrum in Fig. 2 between 335 and 343 mT as shown in Fig. 3. An excellent fit to this region is found by including a feature due to dangling bonds with a g value of 2.005 shown in red, a line due to conduction electrons with a g value of 2.003 shown in blue, and the hyperfine line due to isolated sodium atoms with a g value of 1.999 shown in gray. There is a small feature in the experimental data just above 339 mT in Fig. 3, which was not reproducible in other measurements and samples. This fit allows us to estimate the spin density associated with the hyperfine and free-carrier lines based on the observation that the temperature dependence of the intensity of the line due to dangling bonds follows a paramagnetic Curie law. That is, while the measured intensity of the dangling bond feature changes, the total number of spins contributing to the line

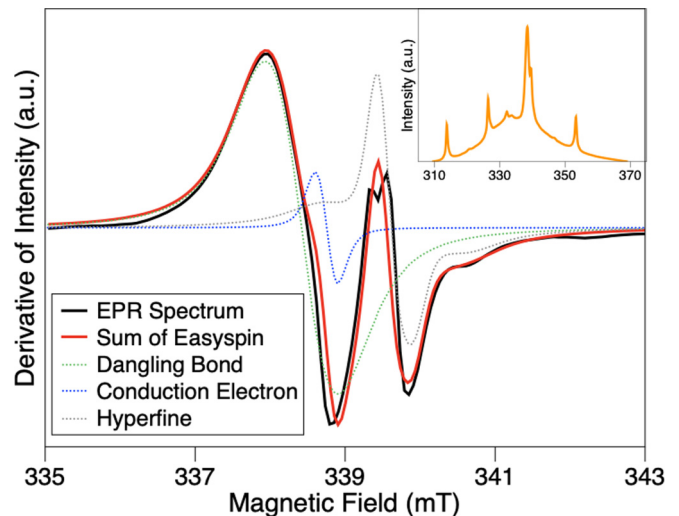


FIG. 3. EPR spectrum of type-II Si clathrates with low Na concentration at 10 K, showing the three features computed in the EASYSIN [28] fitting and the sum of the three features compared to experiment. The inset shows the integrated spectrum over all fields (EPR spectrum shown in Fig. 2), clearly showing the broad feature attributed to Na clustering.

remains roughly constant [22] (intensity saturation due to excessive microwave power at these temperatures was shown to introduce an error of at most a factor of 2). This observation allows the room-temperature spin density results for the dangling bonds to be used as a reference in calibrating the integrated intensities of the other features. With this method, we find a spin density of $\sim 4 \times 10^{17} \text{ cm}^{-3}$ for the isolated Na atoms, with each hyperfine line contributing roughly the same amount to the total spin density. This estimate is an average which assumes isolated Na atoms are spread uniformly across the sample. Depending on the size of the disordered silicon phase, for example, the actual density could be larger.

The inset in Fig. 3 shows an integral of the 10-K EPR spectrum. The broad peak centered at a slightly lower field than the dangling bond line has been previously observed and associated with clustered Na [3,5]. The area of the broad feature in our sample is roughly $10 \times$ larger than the area in the four hyperfine lines. This allows us to estimate the total Na concentration is $\sim 5 \times 10^{18} \text{ cm}^{-3}$. This is a regime where the clathrate can be viewed as a heavily doped semiconductor. Using this Na concentration, the size of the type-II Si clathrate unit cell, and assuming the Na is uniformly distributed in the large cages, we find the probability a large cage is filled is ~ 0.002 and estimate $x \sim 0.016$ in $\text{Na}_x\text{Si}_{136}$.

With the information on Na in Si clathrates, it is interesting to compare its properties to other shallow donors, such as phosphorus (P) in crystalline silicon ($c\text{-Si}$). The binding energy of Na in clathrates has been estimated at around 10 meV [13], consistent with our measurements of the temperature dependence of the intensity of the hyperfine lines, whereas the binding energy of P in $c\text{-Si}$ is around 40 meV [39,40]. At the same time, the density of the donor wave function at the nucleus for P in $c\text{-Si}$ [$|\Psi_P(r=0)|^2 \approx 1-4 \times 10^{29} \text{ m}^{-3}$ [39]] is 5 to 10 times smaller than what is estimated for Na in clathrates

$[\Psi_{\text{Na}}(r=0)]^2 \approx 2 \times 10^{30} \text{ m}^{-3}$ [20]]. The decreased density at the nuclear site is in part attributable to the dielectric constant playing a larger role in the substitutional P atom, whereas the open, cagelike structure around the interstitial Na atom has been interpreted to mean the dielectric constant should have a negligible role at distances shorter than the radius of the cage [4]. The larger effective dielectric constant for P in *c*-Si then leads to a larger Bohr radius [40,41] than for Na in clathrates. In a simple hydrogenic model, the spatial extent of the wave functions and corresponding binding energies may seem inconsistent. However, a model of Na donors in clathrates given by Sim *et al.* [20] used a muffin-tin potential and found spatial extents of the wave function consistent with EPR estimates. Their model also predicts a binding energy of about 90 meV which, though larger than EPR estimates, is consistent with the view of Na as a shallow donor.

The differences between the two shallow donors are manifest in their respective EPR spectra. The EPR spectrum of P in *c*-Si exhibits two hyperfine lines, attributed to the spin- $\frac{1}{2}$ P nucleus, surrounding a conduction electron line [42]. The hyperfine splitting is 41 G, about 1.1% of the splitting of a free P atom of 3640 G [34,35]. The same number for Na in clathrates is about 42%. The smaller splitting for P in *c*-Si compared to Na in clathrates is attributable to its reduced density at the donor nucleus as well as the smaller magnetic moment of the donor nucleus. Despite these similarities, *c*-Si:P has a much lower critical density for the metal-insulator transition ($\sim 10^{18} \text{ cm}^{-3}$ [41]) than Na in clathrates ($\sim 10^{21} \text{ cm}^{-3}$ [4,12,19]) due to the smaller extension of the Na donor wave function onto the surrounding silicon lattice. In comparing potential applications of P and Na donors in modern research, while P in *c*-Si has garnered significant attention in the topic of solid-state spin qubits, the distinct properties of Na donors in Si clathrates may make it an interesting alternative for future exploration in this subject.

Returning to the inset to Fig. 3, based on the presence of both isolated Na and the broad feature due to clustered Na, it has been suggested that the Na is not uniformly distributed [4,5,14]. In addition, several studies have argued that it may be energetically favorable to form Na-Na dimers [19,31]. In this context, it is interesting to examine whether the relative areas of the isolated Na and two Na EPR lines are consistent with a random distribution. Using the EASYSYSPIN fits, the ratio of the integrated intensity of the two Na lines to the isolated Na

lines is about 10%. If we assume the two Na lines arise solely from Na atoms on next-nearest-neighbor large cage sites, we can use the occupation probability given above to estimate this ratio would be an order of magnitude lower than observed.

Alternatively, we can assume the Na is randomly distributed and ask what the observed two Na to one Na intensity ratio implies about how far away from a given Na a neighboring Na can be and still contribute to the two Na line. This analysis has been developed for P in diamond Si where analogous isolated P, P pair, and clustered P lines have been characterized [36,37,43,44]. The question essentially becomes one of the extent of the donor wave function which determines how far apart two Na atoms can be and still have an exchange energy sufficient to contribute to the two Na line. Following the approaches of Ref. [44], we find that Na atoms with separations up to $\sim 20 \text{ \AA}$ would need to contribute to account for the measured ratio. This would indicate third- and even fourth-nearest neighbors are contributing to the paired line. The spatial extent of the donor wave function onto neighboring sites found above coupled with the fact that J needed to be comparable to or larger than the Zeeman energy to fit the two Na features would argue against such contributions. While not definitive, this again suggests the distribution is not random. The fact that the linewidth of the two Na line is comparable to the isolated Na line could be taken as additional support since we might expect broadening if a broad range of sites and J values contributed to the two Na feature.

The presence of the conduction electron peak in the low-temperature spectrum provides additional evidence that the Na distribution is not random. The intensity of the peak drops more than an order of magnitude from room temperature to 10 K, consistent with localization of carriers on the Na atoms. The fact that the peak is still present at 10 K, however, indicates local regions of the sample still have sufficiently high Na concentration to form an impurity band. The same conclusion of an inhomogeneous Na distribution was reached in Ref. [29] in their analysis of guest displacement and dimerization of Na.

The mechanisms through which an inhomogeneous Na distribution or Na clustering might arise are not clear at the moment. Such an effect could be driven by an attractive interaction between Na atoms at low concentration as mentioned earlier [19] or the energetics of the diffusion process [12]. For example, diffusion of Na out of type-II clathrate is known

TABLE I. Estimated spin densities and g values obtained via the methods described in the text. HF1 refers to the hyperfine lines resulting from a single Na nucleus, and HF2 refers to hyperfine lines resulting from a pair of Na nuclei. Data for dangling bonds (DB) and free carriers (FC) at room temperature are obtained directly from experiment, while the others are obtained from integration of EASYSYSPIN fits to the experimental spectra. g_{\perp} refers to the effective g value perpendicular to the applied magnetic field, and g_{\parallel} refers to the effective g value parallel to the applied field.

	DB	FC (300 K)	FC (10 K)	HF1 (10 K)	HF2 (10 K)
Spin density (cm^{-3})	2×10^{17}	2×10^{17}	1×10^{16}	4×10^{17}	3×10^{16}
g value	2.005	2.003	2.0032	$g_{\perp} = 2.0385$ $g_{\parallel} = 2.0360$	$g_{\perp} = 2.0385$ $g_{\parallel} = 2.0360$

to involve Na moving from small to large cages [12]. If Na were more likely to fill an empty large cage when a neighboring large cage is occupied, this could drive clustering. The HF/HNO₃ etch step could also affect inhomogeneity. In diamond silicon, this etch has a rate with a strong dependence on dopant concentration [21] although generally the etch rate is higher for higher doping, which might tend to remove clusters.

As a reference, the spin densities and g values at room temperature and 10 K for all of the EPR lines discussed here are summarized in Table I.

IV. CONCLUSION

We have confirmed the source of two lines in the silicon clathrate EPR spectrum that have not been well understood in previous reports. The first is a line due to dangling bonds at $g = 2.005$, which we speculate arises from a disordered phase which surrounds each grain in the powder and hence dominates the transport across the powder. The identification of this line supports the theory provided by Mott of the thermally activated hopping behavior observed in clathrate powders. Hence, future studies of silicon clathrate powders must take into account the effects of these defects.

The second is a superhyperfine doublet arising from the interaction of the Na donor electron with naturally occurring

²⁹Si on the Si cage. Furthermore, our analysis of the hyperfine interactions with ²³Na and ²⁹Si provides confirmation that Na is a shallow dopant with the spatial extent of its electronic state extending beyond the cage in which the Na resides. These results also suggest, however, that the Na wave function is not that of a simple hydrogenic donor. We have also discussed similarities and differences between the EPR spectrum of P in diamond silicon and Na in Si clathrates. The former has received considerable recent attention for its potential application as a spin qubit. Some of the differences between these two donors, including the larger hyperfine coupling and smaller Bohr radius of Na in type-II clathrate, may warrant further investigation of this system for its potential as an alternative solid-state spin qubit.

We also find evidence that the distribution of Na atoms resulting from common type-II Si clathrate preparations may be inhomogeneous. This issue will need to be understood and controlled if the Na-doped Si₁₃₆ allotrope is to find applications as a Si-based semiconductor.

ACKNOWLEDGMENTS

The authors thank Dr. X. Steier and C. Pierce for their help with the PECVD system. This work was supported by the National Science Foundation, Grant No. 1810463.

W.K.S. and Y.L. contributed equally to this work.

-
- [1] J. S. Kasper, P. Hagenmuller, M. Pouchard, and C. Cros, Clathrate structure of silicon Na₈Si₄₆ and Na_xSi₁₃₆ ($x < 11$), *Science* **150**, 1713 (1965).
- [2] C. Cros, M. Pouchard, and P. Hagenmuller, Sur une nouvelle famille de clathrates minéraux isotopes des hydrates de gaz et de liquides. interprétation des résultats obtenus, *J. Solid State Chem.* **2**, 570 (1970).
- [3] L. Krishna, L. L. Baranowski, A. D. Martinez, C. A. Koh, P. C. Taylor, A. C. Tamboli, and E. S. Toberer, Efficient route to phase selective synthesis of Type II silicon clathrates with low sodium occupancy, *CrystEngComm* **16**, 3940 (2014).
- [4] N. Mott, Properties of compounds of type Na_xSi₄₆ and Na_xSi₁₃₆, *J. Solid State Chem.* **6**, 348 (1973).
- [5] A. Ammar, C. Cros, M. Pouchard, N. Jaussaud, J.-M. Bassat, G. Villeneuve, M. Duttine, M. Ménérier, and E. Reny, On the clathrate form of elemental silicon, si136: preparation and characterisation of Na_xSi₁₃₆ ($x \rightarrow 0$), *Solid State Sci.* **6**, 393 (2004).
- [6] V. I. Smelyansky and J. S. Tse, The electronic structure of metallo-silicon clathrates Na_xSi₁₃₆ ($x = 0, 4, 8, 16$ and 24), *Chem. Phys. Lett.* **264**, 459 (1997).
- [7] A. D. Martinez, L. Krishna, L. L. Baranowski, M. T. Lusk, E. S. Toberer, and A. C. Tamboli, Synthesis of group iv clathrates for photovoltaics, *IEEE J. Photovolt.* **3**, 1305 (2013).
- [8] L. Grigorian, P. Eklund, and S. Fang, U. S. Patent No. 6 103 403, Aug. 2000.
- [9] G. B. Adams, M. O’Keeffe, A. A. Demkov, O. F. Sankey, and Y.-M. Huang, Wide-band-gap si in open fourfold-coordinated clathrate structures, *Phys. Rev. B* **49**, 8048 (1994).
- [10] A. A. Demkov, O. F. Sankey, K. E. Schmidt, G. B. Adams, and M. O’Keeffe, Theoretical investigation of alkali-metal doping in Si clathrates, *Phys. Rev. B* **50**, 17001 (1994).
- [11] J. Gryko, P. F. McMillan, R. F. Marzke, G. K. Ramachandran, D. Patton, S. K. Deb, and O. F. Sankey, Low-density framework form of crystalline silicon with a wide optical band gap, *Phys. Rev. B* **62**, R7707(R) (2000).
- [12] G. K. Ramachandran, J. Dong, J. Diefenbacher, J. Gryko, R. F. Marzke, O. F. Sankey, and P. F. McMillan, Synthesis and x-ray characterization of silicon clathrates, *J. Solid State Chem.* **145**, 716 (1999).
- [13] H. Yahiro, K. Yamaji, M. Shiotani, S. Yamanaka, and M. Ishikawa, An ESR study on the thermal electron excitation of a sodium atom incorporated in a silicon clathrate compound, *Chem. Phys. Lett.* **246**, 167 (1995).
- [14] S. B. Roy, K. E. Sim, and A. D. Caplin, The insulator-to-metal transition in Si-Na ‘clathrate’ compounds: A search for superconductivity, *Philos. Mag. B* **65**, 1445 (1992).
- [15] M. Beekman, C. P. Sebastian, Y. Grin, and G. S. Nolas, Synthesis, crystal structure, and transport properties of Na₂₂Si₁₃₆, *J. Electron. Mater.* **38**, 1136 (2009).
- [16] M. Beekman, W. Schnelle, H. Borrmann, M. Baitinger, Y. Grin, and G. S. Nolas, Intrinsic Electrical and Thermal Properties from Single Crystals of Na₂₄Si₁₃₆, *Phys. Rev. Lett.* **104**, 018301 (2010).
- [17] M. Beekman, M. Baitinger, H. Borrmann, W. Schnelle, K. Meier, G. S. Nolas, and Y. Grin, Preparation and crystal growth of Na₂₄Si₁₃₆, *J. Am. Chem. Soc.* **131**, 9642 (2009).

- [18] S. Stefanoski, M. Beekman, W. Wong-Ng, P. Zavalij, and G. S. Nolas, Simple approach for selective crystal growth of intermetallic clathrates, *Chem. Mater.* **23**, 1491 (2011).
- [19] S. Stefanoski, C. D. Malliakas, M. G. Kanatzidis, and G. S. Nolas, Synthesis and structural characterization of $\text{Na}_x\text{Si}_{136}$ ($0 < x \leq 24$) single crystals and low-temperature transport of polycrystalline specimens, *Inorg. Chem.* **51**, 8686 (2012).
- [20] K. E. Sim, Experimental studies of sodium-silicon clathrate compounds, Ph.D. thesis, University of London, 1983.
- [21] V. Raineri, V. Privitera, W. Vandervorst, L. Hellemans, and J. Snauwaert, Carrier distribution in silicon devices by atomic force microscopy on etched surfaces, *Appl. Phys. Lett.* **64**, 354 (1994).
- [22] J.-K. Lee and E. A. Schiff, Modulated Electron-Spin-Resonance Measurements and Defect Correlation Energies in Amorphous Silicon, *Phys. Rev. Lett.* **68**, 2972 (1992).
- [23] S. Zafar and E. A. Schiff, Hydrogen-mediated model for defect metastability in hydrogenated amorphous silicon, *Phys. Rev. B* **40**, 5235 (1989).
- [24] M. Stutzmann and D. K. Biegelsen, Electron-spin-lattice relaxation in amorphous silicon and germanium, *Phys. Rev. B* **28**, 6256 (1983).
- [25] See Supplemental Material at <http://link.aps.org/supplemental/10.1103/PhysRevB.101.245204> for effect of HF/HNO₃ etch on the clathrate sample shown in Fig. S1. Comparison of two outer hyperfine lines shown in Fig. S2. Time-dependent effect on the spectra shown in Fig. S3. Probability distribution of ²⁹Si on the large cage and details of the simulation listed in Table S1.
- [26] H. M'saad, J. Michel, J. J. Lappe, and L. C. Kimerling, Electronic passivation of silicon surfaces by halogens, *J. Electron. Mater.* **23**, 487 (1994).
- [27] E. Michel, T. Pauly, V. Eteläniemi, and G. Materlik, Adsorption of I on Si(111) and Si(110) surfaces, *Surf. Sci.* **241**, 111 (1991).
- [28] S. Stoll and A. Schweiger, Easyspin, a comprehensive software package for spectral simulation and analysis in EPR, *J. Magn. Reson.* **178**, 42 (2006).
- [29] F. Tournus, B. Masenelli, P. Mélinon, D. Connétable, X. Blase, A. M. Flank, P. Lagarde, C. Cros, and M. Pouchard, Guest displacement in silicon clathrates, *Phys. Rev. B* **69**, 035208 (2004).
- [30] A. D. Ritchie, M. A. MacDonald, P. Zhang, M. A. White, M. Beekman, J. Gryko, and G. S. Nolas, X-ray absorption spectroscopy studies of local structure and electronic properties of $\text{Na}_x\text{Si}_{136}$ ($0 < x < 24$) clathrates, *Phys. Rev. B* **82**, 155207 (2010).
- [31] F. Brunet, P. Mélinon, A. San Miguel, P. Kéghélian, A. Perez, A. M. Flank, E. Reny, C. Cros, and M. Pouchard, Peierls or Jahn-Teller effect in endohedrally doped silicon clathrates: An EXAFS study, *Phys. Rev. B* **61**, 16550 (2000).
- [32] M. Beekman, E. N. Nenghabi, K. Biswas, C. W. Myles, M. Baitinger, Y. Grin, and G. S. Nolas, Framework contraction in Na-stuffed Si(cF136), *Inorg. Chem.* **49**, 5338 (2010).
- [33] E. Abe, A. M. Tyryshkin, S. Tojo, J. J. L. Morton, W. M. Witzel, A. Fujimoto, J. W. Ager, E. E. Haller, J. Isoya, S. A. Lyon, M. L. W. Thewalt, and K. M. Itoh, Electron spin coherence of phosphorus donors in silicon: Effect of environmental nuclei, *Phys. Rev. B* **82**, 121201(R) (2010).
- [34] P. B. Ayscough, *Electron Spin Resonance in Chemistry* (Methuen and Co., London, 1967).
- [35] P. Atkins and M. Symons, *The Structure of Inorganic Radicals* (Elsevier, Amsterdam, 1967).
- [36] P. R. Cullis and J. R. Marko, Determination of the donor pair exchange energy in phosphorus-doped silicon, *Phys. Rev. B* **1**, 632 (1970).
- [37] S. Shankar, A. M. Tyryshkin, and S. A. Lyon, ESR measurements of phosphorus dimers in isotopically enriched ²⁸Si silicon, *Phys. Rev. B* **91**, 245206 (2015).
- [38] S. Yamanaka, M. Komatsu, M. Tanaka, H. Sawa, and K. Inumaru, High-pressure synthesis and structural characterization of the Type II clathrate compound $\text{Na}_{30.5}\text{Si}_{136}$ encapsulating two sodium atoms in the same silicon polyhedral cages, *J. Am. Chem. Soc.* **136**, 7717 (2014).
- [39] H. Hui, An improved effective-mass-theory equation for phosphorus doped in silicon, *Solid State Commun.* **154**, 19 (2013).
- [40] C. Kittel, in *Introduction to Solid State Physics*, 8th ed. (Wiley, Hoboken, NJ, 2005), Chap. 8, pp. 209–210
- [41] T. F. Rosenbaum, R. F. Milligan, M. A. Paalanen, G. A. Thomas, R. N. Bhatt, and W. Lin, Metal-insulator transition in a doped semiconductor, *Phys. Rev. B* **27**, 7509 (1983).
- [42] R. C. Fletcher, W. A. Yager, G. L. Pearson, and F. R. Merritt, Hyperfine splitting in spin resonance of group v donors in silicon, *Phys. Rev.* **95**, 844 (1954).
- [43] G. Feher, R. C. Fletcher, and E. A. Gere, Exchange effects in spin resonance of impurity atoms in silicon, *Phys. Rev.* **100**, 1784 (1955).
- [44] D. New and T. G. Castner, Donor clusters in silicon. results of ESR measurements, *Phys. Rev. B* **29**, 2077 (1984).